

Spectral functions and optical conductivity of spinless fermions on a checkerboard lattice

F. Pollmann, P. Fulde

*Max-Planck-Institut für Physik komplexer Systeme,
Nöthnitzer Strasse 38, 01187 Dresden, Germany*

E. Runge

*Technische Universität Ilmenau, Fakultät für Mathematik und Naturwissenschaften,
FG Theoretische Physik I, 98693 Ilmenau, Germany*

We study the dynamical properties of spinless fermions on the checkerboard lattice. Our main interest is the limit of large nearest-neighbor repulsion V as compared with hopping $|t|$. The spectral functions show broad low-energy excitation which are due to the dynamics of fractionally charged excitations. Furthermore, it is shown that the fractional charges contribute to the electrical current density.

I. INTRODUCTION

Excitations with fractional charge have fascinated physicists for some time. An early investigation by Su, Schrieffer and Heeger¹ dates back to 1979 and deals with the chain molecule trans-polyacetylene $(\text{CH})_n$. This polymer has two ground states A and B with alternating single and double bonds between C atoms. In one of them the double bond is on the right side of a given C atom while in the other ground state it is on the left side. A soliton or kink excitation has the property of an interface between the two ground states, i.e., on one side of the soliton we have alternating bonds like in ground state A and on the other side the bonds are arranged like in ground state B. Shifting the soliton along the chain does not change the energy. Su et al. showed that depending on the occupational number of the kink state which can be either empty, singly or doubly occupied, the excitation has a spin or charge only. In other words, there exist excitations with spin-charge separation but no excitations with fractional charge yet. This changes when trans-polyacetylene is heavily doped. It turns out that at certain doping concentrations of either particles or holes there are not only excitations with charge and spin separated but their charge is a fraction ν of the electronic charge e only.² In the simplest case $\nu = \pm 1/3, \pm 2/3$ etc. It should be mentioned that this phenomenon does not require interactions between electrons but occurs within a single- (or independent) particle description. It involves lattice degrees of freedom though, since a double C = C bond has a different length than a single C – C bond. Doped trans-polyacetylene serves as an example of a one-dimensional system with fractional charges.

Fractional charges are also found in two dimensions in the much celebrated fractional quantum Hall effect (FQHE). It was Laughlin³ who introduced this concept here. He explained with it the behavior of electrons in high-quality GaAs/AlGaAs heterostructures in an applied magnetic field B normal to the planes. When the field deviates slightly from $B = nhc/e\nu$, where n is the density of the electrons and ν is a rational frac-

tion with odd denominator, excitations with charge $\pm\nu e$ occur. As usual h is Planck's constant. The excitations with fractional charge νe are based on a new type of correlated ground state called the Laughlin state. It has been also demonstrated that the excitations fulfill fractional statistics, i.e., when two of them are exchanged the phase changes by $e^{i\nu\pi}$. In distinction to the previously considered trans-polyacetylene, electron-electron interactions are crucial here. In an applied magnetic field, correlations become strong since the kinetic energy of the electrons is reduced.

The question was left open whether or not fractionally charged excitations exist in two or three dimensional systems without magnetic fields. In Ref. [4] it was suggested that in a pyrochlore lattice, a prototype of a three dimensional structure with geometrical frustration, excitations with charge $e/2$ do exist. The pyrochlore structure is found, for example, in the transition metal compound LiV_2O_4 . In that compound, vanadium has a half-integer valency and electronic correlations are strong as indicated by a large γ coefficient in the low temperature specific heat $C = \gamma T$. Although LiV_2O_4 has motivated work of the kind presented here, we do not claim that the theory of fractional charges applies to that specific material. Generally, prerequisites for fractional charges in the considered model are strong short-range correlations and certain band fillings. In order to study a system of this sort in more detail, a checkerboard lattice is considered which also allows for numerical investigations. The checkerboard lattice can be thought of as a projection of the pyrochlore lattice onto a plane. Although there are differences in the physics of the two systems due to the different dimensions, one can learn much from the simpler two dimensional system. Numerous studies of the pyrochlore and checkerboard lattice were done and reported in Refs. [5,6,7,8] for spin degrees of freedom and [9,10,11] for charge degrees of freedom. The question has not been posed yet how one would be able to detect these excitations with fractional charges in case they exist. It is the purpose of the present investigation to shed some light on that topic by calculating spec-

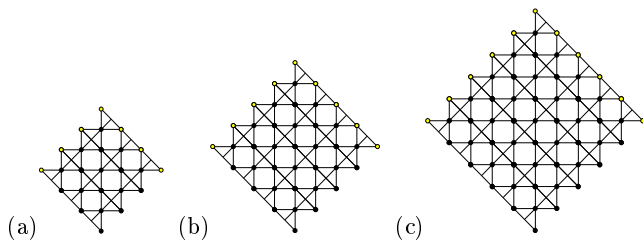


Figure 1: Checkerboard lattice (periodic boundary conditions are used for the calculations). Lattices with (a) 18 sites, (b) 32 sites and (c) 50 sites are considered.

tral functions and optical conductivity of fully spin polarized or, equivalently, spinless fermions on a checkerboard lattice. It is demonstrated that the fractionalization of charge leads to characteristic features which are absent when fractionalization is forbidden. Perhaps the present investigation may sharpen the attention of experimentalists when doing photoemission experiments on, e.g., systems with spinel structure when the filling factors are right. Also the experimental progress in the generation of optical lattices should be noted. Recently it has been reported that 3D optical lattices can be generated and filled with either bosons or fermions to simulate relevant Hamiltonians, e.g., in Ref. [12] and citations therein.

The paper is organized as follows. First we introduce in Section II the model Hamiltonian that is used for our calculations and show how under certain conditions fractionally charged particles (fcp's) arise on a checkerboard lattice. In Section III, we briefly discuss the numerical details and introduce the approximations we applied. The calculated spectral functions and optical conductivities are presented in Section IV. Finally, the results and conclusions are summarized in Section V.

II. HAMILTONIAN AND LATTICES

The model Hamiltonian

$$H = -t \sum_{\langle i,j \rangle} (c_i^\dagger c_j + \text{h.c.}) + V \sum_{\langle i,j \rangle} n_i n_j \quad (1)$$

describes spinless fermions on a checkerboard lattice (see Fig. 1) with nearest-neighbor hopping amplitude t and nearest-neighbor repulsion V . The operators c_i (c_i^\dagger) annihilate (create) a particle on site i . The density operator is $n_i = c_i^\dagger c_i$. To avoid boundary effects, which are expected to be strong, we choose periodic boundary conditions in actual calculations.

The band structure of non-interacting ($V = 0$) particles on the crisscrossed checkerboard lattice consists of a

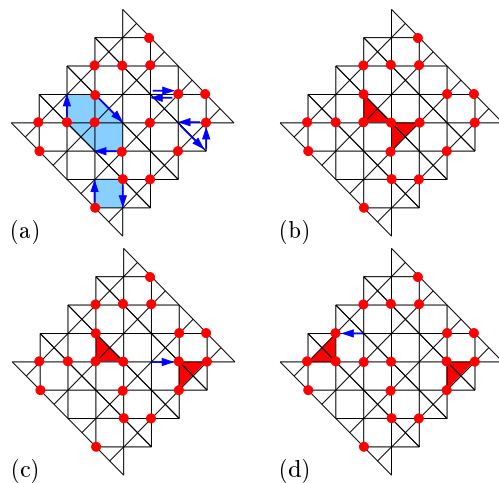


Figure 2: (color online) (a) Example of an allowed configuration of a checkerboard lattice at half filling with possible low-order hopping processes. (b)-(d) Adding one particle leads to two mobile defects, marked by triangles. Arrows mark motions of particles.

dispersive and a flat band

$$\begin{aligned} \varepsilon^-(\mathbf{k}) &= -2t - 4t \cos \frac{k_x a}{\sqrt{2}} \cos \frac{k_y a}{\sqrt{2}} \\ \varepsilon^+(\mathbf{k}) &= 2t, \end{aligned} \quad (2)$$

where a is the lattice constant. In passing, we mention that in the presence of interactions correlations are generally strong in the flat band regimes. The kinetic energy does not counteract optimization of repulsions in that regime.¹³ In the following we assume $t > 0$. Note that our coordinate system is rotated by 45° relative to that of, e.g., Ref. [14]. The resulting difference in boundary conditions can lead to noticeable numerical differences in particular for very small cluster sizes.

Our main interest is in the regime $t/V \ll 1$, at half filling. When $t = 0$ the ground state manifold is macroscopically degenerate: Every configuration with exactly two particles on each crisscrossed square is a ground state. This is the two dimensional equivalent of the tetrahedron rule¹⁵ (or Anderson rule). We refer to configurations fulfilling the tetrahedron rule as “allowed configurations”. The macroscopic degeneracy is lifted for small but finite hopping amplitude t .

In the following we discuss processes up to order t^3/V^2 . They can be classified as self-energy contributions and ring exchanges (see Fig. 2(a)). The self-energy contributions are identical for all allowed configurations and therefore the ground state degeneracy is not lifted by them. The total amplitude of ring exchange around empty squares is proportional to t^2/V and vanishes for fermions. However, the macroscopic degeneracy is lifted by ring exchanges $\sim t^3/V^2$ around hexagons. Note that for fermions the signs of the corresponding matrix elements depend on the sequence in which the sites are

enumerated.¹⁴

Placing one additional particle with charge e onto an empty site leads to a violation of the tetrahedron rule on two adjacent crisscrossed squares (see Fig. 2(b)). The energy is increased by $4V$ since the added particle has four nearest-neighbors. Particles on a crisscrossed square with three particles can hop to another crisscrossed square without creating more violations of the tetrahedron rule, i.e., without increase of repulsive energy (see panels (c) and (d) in Fig. 2). By these processes, two local defects (violating the tetrahedron rule) can separate over large distances thereby gaining additional kinetic energy of order t . This is observed in our calculations. We will see below in the context of Fig. 3 that the bandwidth from an artificially restricted calculation in which the defects are not allowed to separate is much smaller than that from the unrestricted calculation.

These findings motivate the introduction of the following effective Hamiltonian that acts only on the subspace of allowed configurations with a given number of violations (e.g., two violations in Fig. 2 (b)-(d)):

$$H_{\text{eff}} = g \sum_{\{\diamond\}} (-1)^{n_0} \left(\left| \begin{array}{c} \text{fcp} \\ \text{fch} \end{array} \right\rangle \langle \begin{array}{c} \text{fcp} \\ \text{fch} \end{array} | + \left| \begin{array}{c} \text{fch} \\ \text{fcp} \end{array} \right\rangle \langle \begin{array}{c} \text{fch} \\ \text{fcp} \end{array} | + \text{h.c.} \right) - t \sum_{\langle i j \rangle} \mathcal{P} \left(c_i^\dagger c_j + \text{h.c.} \right) \mathcal{P}. \quad (3)$$

It includes the lowest order ring exchange process with $g \sim t^3/V^2$ (compare Ref. 14). We will refer to it as the t-g model. Note that the sign of the matrix elements depends on the configuration, i.e., for row wise enumeration of sites a process has a minus sign whenever the site in the center of the corresponding hexagon is occupied ($n_0 = 1$) and a plus sign when it is empty. The hopping t is projected onto the manifold of allowed configurations plus fixed numbers of violations by the projector \mathcal{P} . By introducing the independent parameters t and g the effect of ring exchange onto the dynamics of fractional excitations can be estimated. The tendency for confinement can be studied even on rather small clusters by increasing the ring exchange strength g .

One can expect that for an infinitely large system the two defects can propagate freely and independently throughout the system. In that case they should be considered as two elementary excitations each having a dispersion $\tilde{\varepsilon}(\mathbf{k}) \sim t$ and each carrying the fractional charge $e/2$. Similarly, the repulsion-energy increase of $4V$ is split between the two elementary excitations. We will refer to these excitations as fractionally charged particles (fcp's). It should be emphasized that they are not quasiparticles in the sense of Landau's Fermi liquid theory because they are not adiabatically connected to independent fermions. Analogously, taking one particle out of the system generates two fractionally charged holes (fch's), i.e., two crisscrossed square with one particle only. Furthermore, quantum fluctuations generate fcp and fch pairs. Starting from an allowed configuration, when one

particle is hopping to an empty neighboring site it creates one crisscrossed square with three particles (fcp) and one crisscrossed square with one particle (fch) only.

Whether or not two defects actually *do* separate completely is a very subtle problem. The answer will depend on lattice type, dimensionality, spin vs. spinless particles, etc. The answer may also differ for zero and finite temperatures T and depend on defect concentration. In any case, the key observation is that whenever two defects with charge $\pm e/2$ separate they change the background configuration. Infinite defect separation (deconfinement) is more plausible for liquidlike ground states than, for ground states with, e.g., broken translational invariance. In the latter case, restoring forces occur which can lead to linear confinement, analogously to quark confinement known from QCD. Thus a thorough analysis of the ground state of the undoped, i.e., half filled system is a vital step towards answering the above questions. First numerical results for an effective model on finite systems up to 64 sites have been presented in Ref. [14]. A two-fold degenerate ground state with stripe order was found for the particular model on the checkerboard lattice. Nevertheless, various observations suggested that it would disappear in the thermodynamic limit. Recent calculations and analytical considerations¹⁶ indicate that this supposition, i.e., that the order would disappear in the thermodynamic limit, was erroneous. The presence of an ordered ground state leads probably to weak confinement of fcp's with a characteristic length of L lattice spacings. A simple estimate is given by $Lg \sim t$, i.e., $L \sim t/g = V^2/t^2$ lattice spacings. For the used parameters, this leads to a large characteristic length of several hundred lattice spacings (weak confinement). Note that the 3D pyrochlore lattice appears at present to have a deconfined phase in which the fcp's can separate^{4,6,17}. The present work focuses on the dynamics of a weakly doped system (half filling plus one extra particle) by calculating the spectral functions and optical conductivity. We stress that the numerical simulations are limited to small clusters. As a consequence, as long as clusters of size $L \sim t/g = V^2/t^2 \gg 1$ are out of reach for the exact diagonalization, we can not hope to find simple finite size scaling relations towards the true thermodynamic limit. The present study should be considered as a contribution towards the understanding of the local behavior of fcp's. In particular it is impossible to distinguish between a free or weakly bound pair of fcp's.

III. NUMERICAL DETAILS

Obviously, conventional approximation schemes such as mean-field theories and Green's function decoupling schemes are not able to describe the strong local correlation expressed by the tetrahedron rule. Furthermore, until now neither a creation operator formalism nor a field theoretical description for the fcp's have been derived. This suggests numerical studies. Unfortunately,

the fact that we are dealing with fermions rules out the use of standard Monte-Carlo techniques. Thus we have chosen the exact diagonalization of the Hamiltonian (1) for small finite lattices, even though the numerical effort increases exponentially with system size.

Diagonalization within the full Hilbert space was done for a lattice containing 18 sites. Larger systems can be considered if we restrict ourselves within the corresponding Hilbert spaces to certain low-energy sectors. They are defined by the number of violations of the tetrahedron rule. For the actual calculations we used the smallest possible Hilbert spaces allowing for the dynamical processes that we are interested in. These consists in the undoped case, i.e, at half filling of the allowed configurations and those with one additional vacuum fluctuation present (one fcp and one fch). In the doped case, i.e, with one particle added to the system, the configurations account for no other violations of the tetrahedron rule than those that are due to the added particle (two fcp's). We refer to the space spanned by these selected configurations as the "minimal Hilbert space" in each case. The dimensions are strongly reduced as compared with the full Hilbert space (see Table I). Calculations for the doped system have

	18 sites	32 sites	50 sites
<i>Half filling</i>			
Full Hilbert space	48 620	601 080 390	1.2641 10 ¹⁴
Allowed states	68	2970	67 832
Minimal (1 fluct.)	2 228	168 858	16 178 232
<i>System doped with one particle</i>			
Full Hilbert space	43 758	565 722 720	1.2155 10 ¹⁴
Minimal (0 fluct.)	1 323	98 784	8 698 450
Confined (0 fluct.)	612	47 520	1 695 800
One extra fluctuation	11 475	2 435 808	-

Table I: Dimensions of the full Hilbert space and some relevant subspaces for different lattice sizes.

also been done for two other subspaces. In one case, the two fcp's subspace is extended to three fcp and one fch in order to check the validity of the results for the two fcp subspace. We refer to this Hilbert space as "one extra fluctuation". In the second case, we confine the two fcp's to adjacent criss-cross squares, i.e., particles do not split into fractional charges. Such calculations have the purpose to demonstrate that charge fractionalization leads to qualitative different behavior.

The spectral functions and optical conductivity of interacting many-particle systems are expectation values of the form

$$G(z) = \langle \psi_0 | A \frac{1}{z - H} A^\dagger | \psi_0 \rangle \quad (4)$$

and can therefore conveniently be calculated numerically by the Lanczos continued fraction method¹⁸ or kernel

polynomial expansion.¹⁹ We found essentially identical results for both algorithms. However, the implementation of the Lanczos method turned out to be slightly faster. We rewrite first $G(z)$ as

$$G(z) = \langle \psi_0 | A A^\dagger | \psi_0 \rangle \langle \phi_0 | \frac{1}{z - H} | \phi_0 \rangle, \quad (5)$$

where

$$|\phi_0\rangle = \frac{A^\dagger |\psi_0\rangle}{\sqrt{\langle \psi_0 | A A^\dagger | \psi_0 \rangle}}. \quad (6)$$

Then the state $|\phi_0\rangle$ is taken as starting vector to generate iteratively with the Lanczos algorithm an orthogonal basis for the Hamiltonian H . Using the tridiagonal form of the Hamiltonian with respect to the Lanczos basis and Kramers' rule, the expectation value can be easily rewritten in terms of diagonal elements a_n and off-diagonal elements b_n of the Hamiltonian in form of a continued fraction

$$G(z) = \frac{\langle \psi_0 | A A^\dagger | \psi_0 \rangle}{z - a_0 - b_1^2 \frac{1}{z - a_1 - b_2^2 \frac{1}{z - a_2 \dots}}}. \quad (7)$$

Well converged results were obtained already after several hundred iterations.

There is, of course, always the question remaining in how far results for finite clusters are indications for the behavior of systems in the thermodynamic limit. Since we cannot go beyond 50 sites, the reader should be cautioned against over interpreting the results.

IV. RESULTS

A. Spectral functions

Direct insight into the dynamics of a many-body system is provided by the spectral function

$$A(\mathbf{k}, \omega) = A^-(\mathbf{k}, \omega) + A^+(\mathbf{k}, \omega), \quad (8)$$

which is the probability for adding (+) or removing (-) a particle with momentum \mathbf{k} and energy ω ($\hbar = 1$) to the system. This function can be directly related to angular-resolved photoemission spectroscopy (ARPES). The particle contribution is defined by

$$A^+(\mathbf{k}, \omega) = \lim_{\eta \rightarrow 0^+} -\frac{1}{\pi} \times \text{Im} \langle \psi_0^N | c_{\mathbf{k}} \frac{1}{\omega + i\eta + E_0 - H} c_{\mathbf{k}}^\dagger | \psi_0^N \rangle \quad (9)$$

and the hole contribution by

$$A^-(\mathbf{k}, \omega) = \lim_{\eta \rightarrow 0^+} -\frac{1}{\pi} \times \text{Im} \langle \psi_0^N | c_{\mathbf{k}}^\dagger \frac{1}{\omega + i\eta - E_0 + H} c_{\mathbf{k}} | \psi_0^N \rangle. \quad (10)$$

Here $|\psi_0^N\rangle$ is the ground state of the system with N particles. A small value of $\eta = 0.1t$ is used for Lorentzian broadening. The operators $c_{\mathbf{k}}$ ($c_{\mathbf{k}}^\dagger$) are obtained from the corresponding operators in real-space representation

$$c_{\mathbf{k}}^\dagger = \frac{1}{\sqrt{N_{\mathbf{k}}}} \sum_j e^{ir_j \mathbf{k}} c_j^\dagger, \quad (11)$$

where $N_{\mathbf{k}}$ denotes the number of \mathbf{k} points in the extended BZ and the sum is taken over all lattice sites. The resulting integrated spectral density is

$$D(\omega) = \frac{1}{N_{\mathbf{k}}} \sum_{\mathbf{k}} A(\mathbf{k}, \omega). \quad (12)$$

For a system with a translationally invariant ground state or if an average over all degenerate ground states is considered, $D(\omega)$ is conveniently calculated in real space representation as a local expectation value

The integrated spectral density $D(\omega)$ for the Hamiltonian (1) is displayed in Fig. 3. The different values of the nearest neighbor repulsion V , show the transition from an independent particle system to the strongly correlated limit. A rather small system is considered in order to allow for a diagonalization in the full Hilbert space with reasonable computational effort. For $V = 0$ the dispersion is given by Eq. 2. $D(\omega)$ includes contributions from the allowed \mathbf{k} -points ($\mathbf{k} = 2\pi/3 (n_x, n_y)$ with $(n_x, n_y) \in \mathbb{Z}^2$). The dispersive band ε^- is completely filled and contributes only to $D^-(\omega)$ while the flat band is empty and contributes exclusively to $D^+(\omega)$.

Adding a particle increases the energy by $4V$. Removing it decreases the repulsion energy by $2V$. Together this leads to an increasing separation of particle and hole part of the spectrum with increasing V and finally to the formation of a gap. By this argument one expects a metal-insulator transition as a function of V . At small but finite V the peaks are broadened as an incoherent background develops. But we are interested in the opposite limit of large V .

In the limit of large V it is sufficient to calculate the spectral functions within the minimal Hilbert space, as is seen from the similarities with results for the full Hilbert space, shown for parameter values $V = 16t$ and $V = 32t$ in Fig. 3. In particular, the bandwidth as well as the gross structure remain unchanged. Therefore we may study much larger systems and compare results for different lattice sizes. In particular, this enables us to approach the question whether the two defects created by injecting one particle are closely bound to each other or not. Unfortunately, calculation on finite clusters can not distinguish truly between free particles and weakly bound pairs. For a first answer, we compare for different lattice sizes the results within the minimal Hilbert space with those from an artificially restricted calculation keeping the two defects confined to two adjacent crisscrossed squares. From Fig. 4 it is seen that without the restriction a broad low-energy continuum is obtained which is missing when the restriction is imposed. The

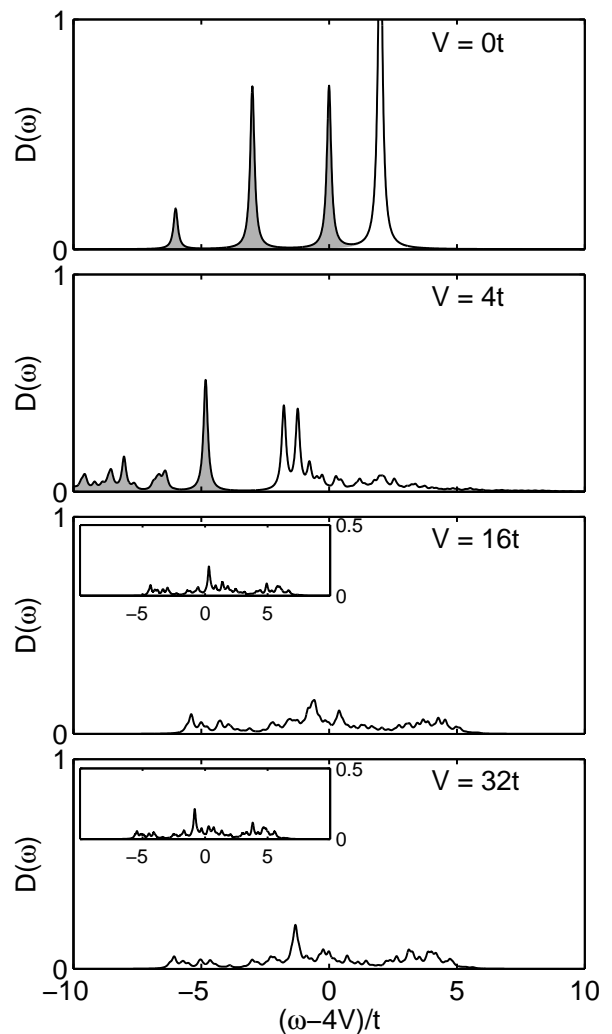


Figure 3: Integrated spectral density $D(\omega)$ of a $\sqrt{18} \times \sqrt{18}$ checkerboard lattice for increasing nearest-neighbor repulsion V . The contributions of $A^-(\mathbf{k}, \omega)$ is shown as shaded area. The insets show $D(\omega)$ calculated for minimal Hilbert spaces. Bandwidths and positions of the dominant features are almost unchanged. The peaks are broadened by choosing $\eta = 0.1t$.

bandwidths are about $13t$ and $8t$ in the two cases. This suggests a simple interpretation. The dynamics of two separate fcp's having a bandwidth of $\approx 6t$ each due to six nearest neighbors would yield the calculated $13t$ while a confined added particle has a much smaller bandwidth, i.e., $8t$. They are rather independent of the system size (e.g., $\approx 13t$ for the 18, 32 and 50 sites cluster in the free case) and therefore expected to extrapolate to the thermodynamic limit. A similar observation holds true for $A^+(\mathbf{k}, \omega)$ (see Fig. 5) where $\mathbf{k} = (0, \pi/2)$ and $\mathbf{k} = (0, \pi)$ are considered. Additionally one observes two interesting facts: (i) The states with large momentum \mathbf{k} give the main contributions to the low-energy continuum in $D(\omega)$. This is consistent with the picture that a particle with large momentum more efficiently lowers its kinetic energy

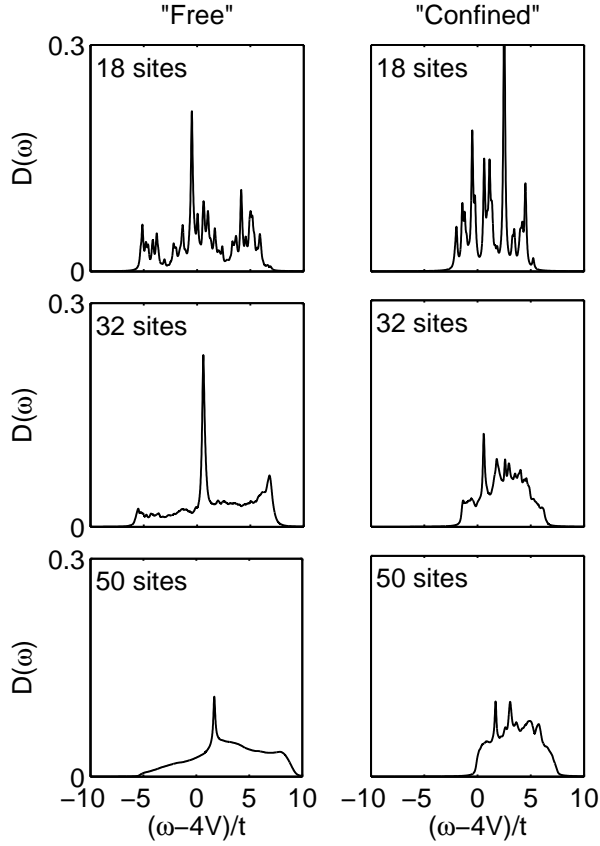


Figure 4: Integrated spectral density $D(\omega)$ for $V = 25t$ calculated for different lattice size. The left panel shows the data from “free” systems which include states with separated fractional charges. The right panel shows the data from systems where the two defect are “confined” and can not separate. The peaks are broadened by choosing $\eta = 0.1t$.

when decaying into fractional excitations than a particle with low momentum. (ii) $A^+(\mathbf{k}, \omega)$ shows in the “confined” calculation a peak-like feature at the low-energy edge that reminds one of the Landau-Fermi liquid peak while nothing alike is seen for the “free” case.

A third observation deserves a comment. For vanishing momentum, the full spectral weight of A^+ is contained in a single sharp δ -like peak near the center of the band. This suggests that $|\tilde{\psi}^{N+1}\rangle = c_{\mathbf{k}=\mathbf{0}}^\dagger |\psi_0\rangle$ is an exact eigenstate of the Hamiltonian H in the limit $t/V \rightarrow 0$ with $\tilde{H}|\tilde{\psi}^{N+1}\rangle = \tilde{E}|\tilde{\psi}^{N+1}\rangle$ as can be seen by evaluation of the following expression:

$$\begin{aligned} H|\tilde{\psi}^{N+1}\rangle &= H c_{\mathbf{k}=\mathbf{0}}^\dagger |\psi_0\rangle \\ &= [H, c_{\mathbf{k}=\mathbf{0}}^\dagger] |\psi_0\rangle + c_{\mathbf{k}=\mathbf{0}}^\dagger H |\psi_0\rangle \\ &= [H, c_{\mathbf{k}=\mathbf{0}}^\dagger] |\psi_0\rangle + E_0 |\tilde{\psi}^{N+1}\rangle. \end{aligned} \quad (13)$$

The contributions of the kinetic and the repulsive energy

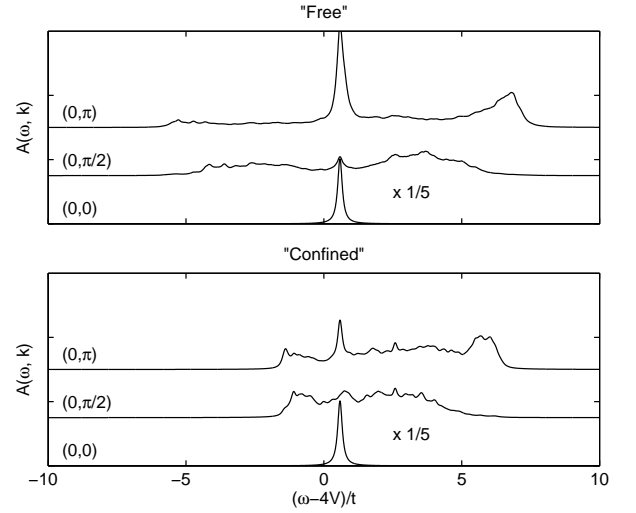


Figure 5: Spectral density $A(\mathbf{k}, \omega)$ for $V = 25t$ calculated for some k -points. The upper panel shows data from the systems which include states with separated fractional charges. The lower panel shows the data from a system where the two defect are “confined” and can not separate. The peaks are broadened by choosing $\eta = 0.1t$.

to the commutator are given by

$$\begin{aligned} [H_{\text{kin}}, c_{\mathbf{k}=\mathbf{0}}^\dagger] &= \left[\sum_{\mathbf{k}'} \varepsilon(\mathbf{k}') c_{\mathbf{k}'}^\dagger c_{\mathbf{k}'} c_{\mathbf{k}=\mathbf{0}}^\dagger \right] \\ &= \varepsilon(\mathbf{k}=\mathbf{0}) c_{\mathbf{k}=\mathbf{0}}^\dagger \end{aligned} \quad (14)$$

and

$$[H_{\text{rep}}, c_{\mathbf{k}=\mathbf{0}}^\dagger] = \frac{V}{\sqrt{N}} \sum_{\langle ij \rangle} (c_j^\dagger n_i + c_i^\dagger n_j), \quad (15)$$

respectively. The latter is calculated by using the real space representation $c_{\mathbf{k}=\mathbf{0}} = 1/\sqrt{N} \sum_l c_l^\dagger$. Since the ground state contains in the considered limit only configurations that obey the tetrahedron rule, each empty site has exactly four occupied neighbors. Thus the sum over all nearest neighbors applied to the ground state leads to

$$\begin{aligned} [H_{\text{rep}}, c_{\mathbf{k}=\mathbf{0}}^\dagger] |\psi_0\rangle &= 4V \frac{1}{\sqrt{N}} \sum_i c_i^\dagger |\psi_0\rangle \\ &= 4V |\tilde{\psi}^{N+1}\rangle. \end{aligned} \quad (16)$$

Collecting everything yields

$$H|\tilde{\psi}^{N+1}\rangle = (\varepsilon(\mathbf{k}=\mathbf{0}) + 4V + E_0) |\tilde{\psi}^{N+1}\rangle. \quad (17)$$

The ground state wave function with one added particle of zero momentum is an eigenfunction of the Hamiltonian with energy $\varepsilon(\mathbf{k}=\mathbf{0}) + 4V + E_0$. Note that for the doped system no vacuum fluctuation is taken into account and thus one has to add a constant energy shift from the self-energy contributions (loss of ground state correlations).

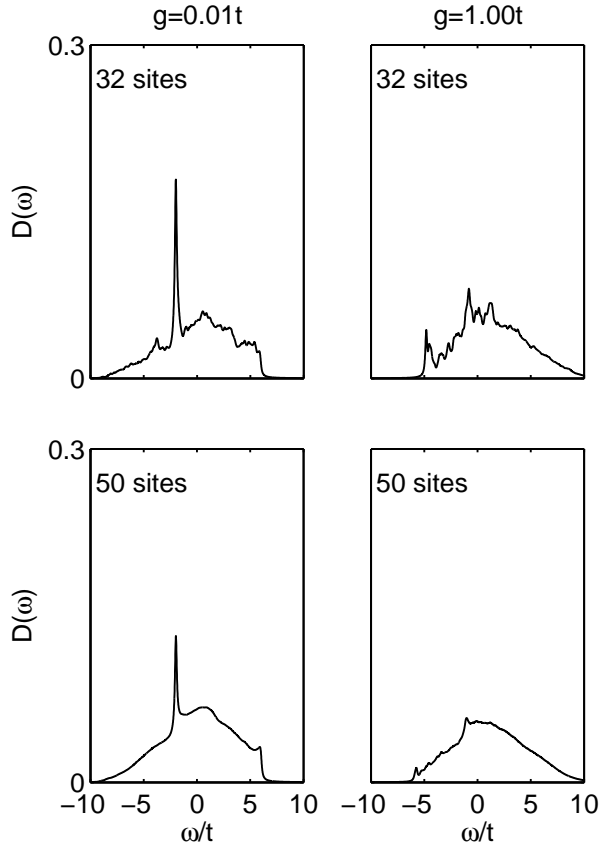


Figure 6: Integrated spectral density of a 32 sites cluster calculated for the effective $t - g$ Hamiltonian for two different values of g . The peaks are broadened by choosing $\eta = 0.1t$.

The integrated spectral density $D(\omega)$ of the effective Hamiltonian (3) shows a strong dependence on the ratio t/g . In the “physical” regime, corresponding to the previously considered parameters with $g \sim t^3/V^2 = 0.01t$, the integrated spectral density $D(\omega)$ (Fig. 6) shows qualitatively the same features as the full Hamiltonian. If g is assumed to be equal to t , the broad continuum at the bottom of the spectral density vanishes and a sharp δ -peak evolves instead. Note the similarities to $D(\omega)$ for the artificially confined situation. The spectral weight of the peak can be looked at as that of a Landau quasiparticle peak. This suggests the interpretation that the ring exchange term leads to charge order which is destroyed by the separation of the two fcp’s. In the regime with $g \ll t$ ($g = t^3/V^2$) the diameter of the two bounded fcp’s is larger than the considered system size and thus the excitations seem to be deconfined. An artificial increased g leads to much stronger confinement and the diameter of the bounded pair is small compared to the system size - leading to a finite weight of the quasiparticle peak. The huge spatial extend of the quasiparticle in the “physical” regime is expected to lead to very interesting effects, but this will be the subject of a separate investigation.

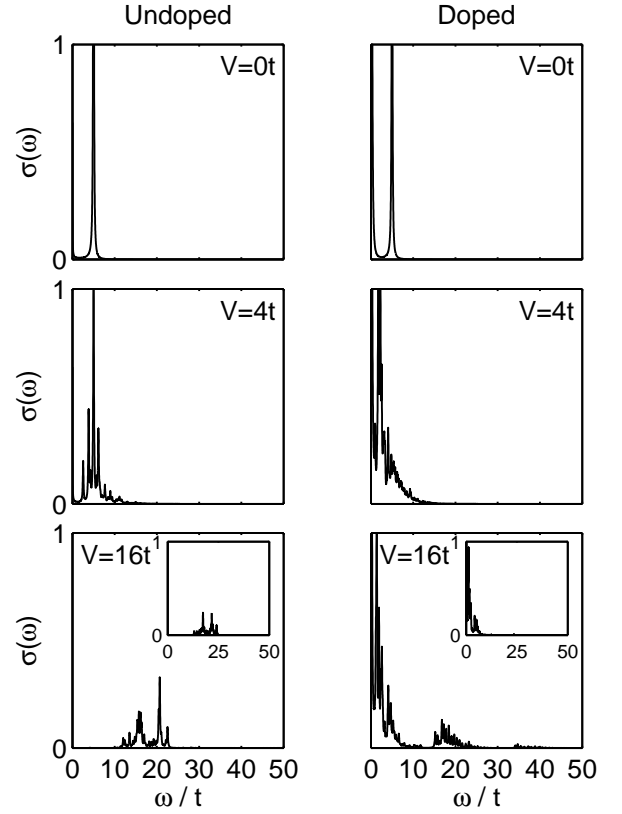


Figure 7: Regular part of optical conductivity $\sigma_{\text{reg}}(\omega)$ of the $\sqrt{18} \times \sqrt{18}$ checkerboard lattice for increasing nearest-neighbor repulsion V . Left panels are showing the half filled case and the right half-filled plus one. The insets show the data for the same values within the minimal Hilbert space. The peaks are broadened by choosing $\eta = 0.1t$.

B. Optical Conductivity

The regular part of the optical conductivity σ_{reg} is defined by

$$\sigma_{\text{reg}}(\omega) = \lim_{\eta \rightarrow 0^+} -\frac{1}{\omega \pi} \times \text{Im} \langle \psi_0^N | j_{\mathbf{x}} \frac{1}{\omega + i\eta + E_0 - H} j_{\mathbf{x}} | \psi_0^N \rangle. \quad (18)$$

Here $|\psi_0^N\rangle$ is the ground state of the system with N particles and as before we use a value of $\eta = 0.1$ for broadening. The current operator is

$$j_{\mathbf{x}} = i[H, X] = it \sum_j \left(c_{\mathbf{r}_j}^\dagger c_{\mathbf{r}_j + \mathbf{x}} - c_{\mathbf{r}_j + \mathbf{x}}^\dagger c_{\mathbf{r}_j} \right). \quad (19)$$

Calculations have been performed for the current density along the x -axis, i.e. $\mathbf{x} = \mathbf{e}_x$ in 19. The regular part of the optical conductivity $\sigma_{\text{reg}}(\omega)$ is shown in Figure 7 for increasing values of the nearest-neighbor repulsion V .

For $V = 0$, one observes a peak-like structure. In the thermodynamic limit it should be positioned at $\omega = 0$ and the shift to $\omega \neq 0$ is a finite size effect. The same holds true for $V=4t$, which is expected to be still in the metallic phase.¹⁴ With increasing V , the structures become broader. In the half-filled (undoped) case the complete weight is moved to larger ω and the Drude weight goes to zero. One expects a transition to an insulating state. For large V the weight is distributed around $\omega = V$. This corresponds to the energy that is needed to generate a fcp-fch pair which carry an electrical current.

In the doped case one finds a different behavior. Finite weight is found at $\omega = 0$ for arbitrarily large values of V and the charge is carried by two fcp's with charge $e/2$ each. A part of the weight is shifted to larger ω where additional fcp - fch pairs are generated as charge carriers. For $V = 16t$ we compare the results based on the calculation in the full Hilbert space with those for the minimal Hilbert space. The features at small ω are reproduced very well, but in the minimal Hilbert space vacuum fluctuations are absent and thus there is no current contributions from fcp-fch pairs.

Now we want to investigate the influence of fractional charges on the optical conductivity (see Fig. 8). The main features are independent of lattice size. For the "free" system one finds a bandwidth of nearly $13t$ which is the same as for the spectral functions. There are sharp peaks superposed onto a broad structure. The "confined" system has a reduced bandwidth of nearly $8t$ and the broad structure is less pronounced. For the 32 sites cluster the contribution near $\omega = 0$ is smaller than for the other two clusters. This is due to the particular shape of the clusters which lead to a lower degeneracy of the ground state than in the 32 sites case.

In Figure 9 the optical conductivity due to *one* moving fcp is shown. Here we keep one of the two fcp's fixed and let only the other one propagate. One observes a Drude peak and broad structure. Except for the Drude peak no other peaks are observed. The bandwidth is reduced to about half of the bandwidth of two fcp's.

V. SUMMARY AND OUTLOOK

We have studied numerically the dynamical properties of spinless fermions on checkerboard lattices and compared the results for different lattice sizes and models. For the full Hamiltonian a broad low-energy continuum is found and no Fermi liquid peak is present, indicating that an added particle decays into two fractionally charged excitations that separate over the whole finite lattice.

Considering the ring exchange g in the effective Hamiltonian as an independent parameter (not fixed to t^3/V^2) allowed us to explore the regime where the fcp separation is small compared to the system size. The spectral function for large g does not show a broad structure and develops instead a sharp peak. The existence of a quasi-

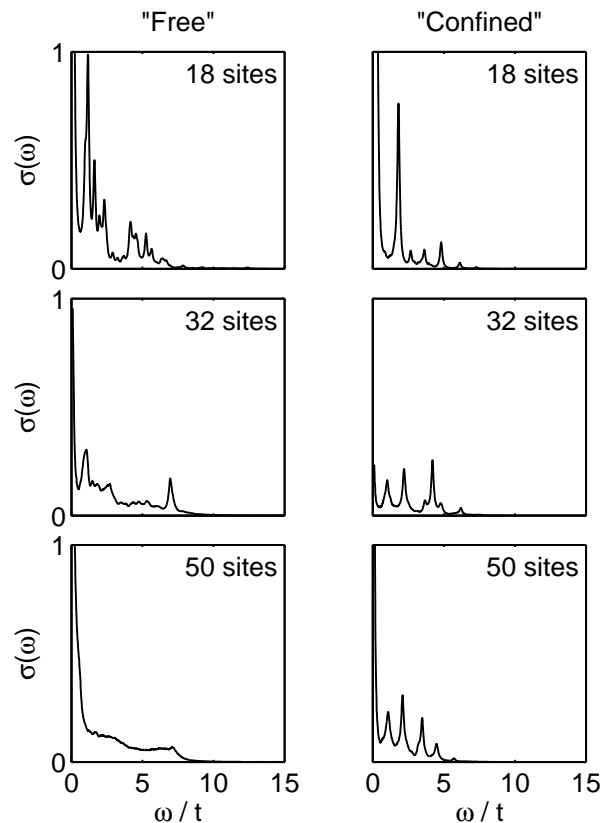


Figure 8: Regular part of optical conductivity $\sigma_{\text{reg}}(\omega)$ for the doped system with $V = 25t$ calculated for different lattice sizes. The left panel shows the data for "Free" systems which include states with separated fractional charges. The right panel shows the data for systems where the two defect are "confined" and can not separate. The peaks are broadened with $\eta = 0.1t$.

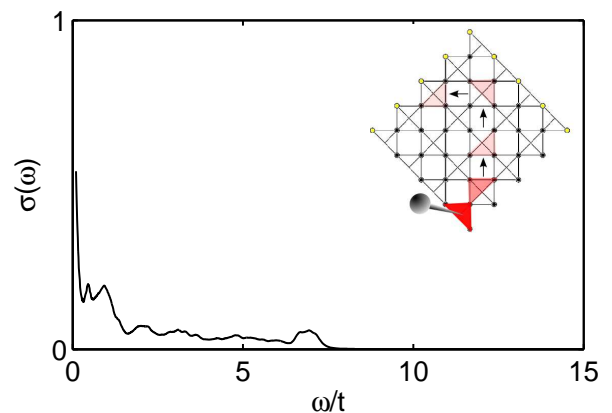


Figure 9: Regular part of optical conductivity $\sigma_{\text{reg}}(\omega)$ for the doped system with $V = 25t$. Only one of the fractional charged excitations is mobile while the other is fixed. The peaks are broadened by choosing $\eta = 0.1t$. Arrows mark motions of particles.

particle peak shows that the added particle creates two bound fractionally charged particles with a small diameter. These findings suggest that for parameters $V/t \approx 10$ quasiparticles with spatial extent over more than hundred lattice sites are formed.

Finally the questions about the dynamics of fractional charges on different types of lattices remains. Considerable differences are expected for bipartite and non-bipartite lattices. Also the dimensionality of the lattice is crucial. For the 3D pyrochlore lattice one speculates about the existence of liquid phases where the fractional charges would be deconfined.^{4,6,17} The informations we got from investigations of finite checkerboard lattices sug-

gest that the possibly deconfined fcp's in the pyrochlore lattice would lead to broad features in spectral functions even for infinite systems.

Acknowledgments

We thank Professor Claire Lhuillier and Professor Joseph Betouras for stimulating discussions and helpful remarks. One author (F. P.) has benefited from the hospitality of IDRIS, Orsay during a stay made possible by a HPC Europe grant (RII3-CT-2003-506079).

-
- ¹ W. P. Su, J. R. Schrieffer, and A. J. Heeger, Phys. Rev. Lett. **42**, 1698 (1979).
² W. P. Su and J. R. Schrieffer, Phys. Rev. Lett. **46**, 738 (1981).
³ R. B. Laughlin, Phys. Rev. Lett. **50**, 1395 (1983).
⁴ P. Fulde, K. Penc, and N. Shannon, Ann. Phys. **11**, 893 (2002).
⁵ G. Misguich and C. Lhuillier, cond-mat p. 0310405 (2003).
⁶ M. Hermele, M. P. A. Fisher, and L. Balents, Phys. Rev. B **69**, 064404 (2004).
⁷ A. Läuchli and D. Poilblanc, Phys. Rev. Letters **92**, 236404 (2004).
⁸ H. T. Diep, ed., *Frustrated Spin Systems* (World Scientific, Singapore, 2005).
⁹ N. Shannon, G. Misguich, and K. Penc, Phys. Rev. B **69**, 220403(R) (2004).
¹⁰ Y. Z. Zhang, M. T. Tran, V. Yushankhai, and P. Thalmeier, Euro. Phys. J. B **44**, 265 (2005).
¹¹ Y. Zhou, Phys. Rev. B **72**, 205116 (2005).
¹² W. Hofstetter, J. I. Chirac, P. Zoller, E. Demler, and M. D. Lukin, Phys. Rev. Lett. **89**, 220407 (2002).
¹³ A. Mielke, J. Phys. A **24**, 3311 (1991).
¹⁴ E. Runge and P. Fulde, Phys. Rev. B **70**, 245113 (2004).
¹⁵ P. W. Anderson, Phys. Rev. **102**, 1008 (1956).
¹⁶ F. Pollmann, J. Betouras, K. Shtengel, and P. Fulde, in preparation (2006).
¹⁷ R. Moessner and S. L. Sondhi, Phys. Rev. B **68**, 184512 (2003).
¹⁸ E. R. Gagliano and C. A. Balseiro, Phys. Rev. Lett. **59**, 2999 (1987).
¹⁹ R. N. Silver, H. Roeder, A. F. Voter, and J. D. Kress, J. Comp. Phys. **124**, 115 (1996).